DOI: 10.1002/ejic.200600052

Polymers or Supramolecules Generated From a New V-Shaped Bis-monodentate Ligand and the Effect of Steric Hindrance on Coordination Modes of the Ligand

Caihua Zhou,[a,b] Yaoyu Wang,*[a] Dongsheng Li,[a,b] Lijun Zhou,[a] Ping Liu,[a] and Qizhen Shi [a]

Keywords: Dipyridylamine / Helical structure / Density functional study / Silver / Copper

A new V-shaped bis-monodentate ligand L (L = 2,3′-dipyridylamine) (**1**) has been designed and synthesized by alkylation reaction of pyridylamine. An investigation of the charge distributions of the coordination atoms and single-point energy calculations of four conformers of ligand L based on the geometry of conformers optimized by the DFT (density functional theory) method was carried out. The results show that the four conformers of ligand L take on two stable and two less stable configurations. Theory forecasts that two relatively stable configurations present in complexes as probable coordination motifs of the ligand, and that steric hindrance of pyridine nitrogen atoms in isomers will affect its coordination ability together with the electronic factor. This forecast has been demonstrated by the coordination chemistry of ligand L, that is, configuration (a) and (b) of the ligand occur in the following reported complexes, which combines with Ag^{I} or Cu^{II} through two coordination modes (bidentate bridging or a monodentate mode) resulting in coordination polymers $\{[Ag(L)_2]NO_3\}_n$ (**2**), $[Cu_2(L)_2(maa)_4]_n$ (maa = methacrylic acid) (**3**), and the mononuclear molecule $[Cu(L)_4](ClO_4)_2 \cdot 2CH_3CH_2OH$ (**4**). The ligand assumes different coordination modes in the three complexes because of different levels of steric hindrance of the pyridine nitrogen atoms in the conformers. Interestingly, polymers **2** and **3** assume a 1D helical structure and a linear framework, respectively, and **4** has a 2D supramolecular architecture induced from hydrogen bond interactions. In addition, the magnetic properties of **3** have been explored, which shows a strong antiferromagnetic interaction.

Introduction

Crystal engineering of coordination polymers and supramolecules have attracted a lot of attention due to their potential as functional materials, as well as their intriguing compositions and topologies. Considerable progress has been made on theoretical forecasting and practical approaches aimed at controlling the topology structure and geometry of the networks.[1–3] However, the general and precise principles for the solid structures of the target products are still subjective because the self-assembly process is highly influenced by several factors such as the structure of ligands, the coordination preference of metal ions, the coordination behavior of counterions, and the solvent system.[4–6] The chemical structure of the organic ligands including the molecular angle, length, and relative orientation of the donor groups plays an extremely important role in dictating polymer topology. So far, much of the research has been concentrated on the exploitation of angular ligands with a molecular angle, such as ligands with a T-shape, V-shape etc, in the construction of versatile coordination polymer architectures.[7–9] Especially, bidentate bridging ligands with a V-shaped structure have been widely used to construct coordination frameworks with a helical structure because of its flexional characteristic and the configuration stability of binding metal ions.[10,11] On the basis of the V-shaped *exo*-bidentate ligand, 2,2′-bis(4-pyridyleneoxy)-1,1′-binaphthalene[12] and 4,4′-oxy-bis(benzoate),[13] several novel helical complexes have been prepared.

With this background in mind, our research has focused on designing new V-shaped ligands and investigating the rational control of their self-assembly with metal centers. In our previous work, we successfully constructed helical structural supramolecular complexes [14] using the V-shaped 3,4′-dipyridylamine ligand. Continuing our investigations on the coordination properties of V-shaped dipyridylamine ligands, we designed another new V-shaped bis-monodentate 2,3′-dipyridylamine ligand. Particularly, this V-shaped molecule is an isomer of the well-documented molecule 2,2′-dipyridylamine, which is widely used as a chelate

[a] Department of Chemistry and Shaanxi Key Laboratory of Physico-inorganic Chemistry, Northwest University, Xi'an 710069, P. R. China
Fax: +86-29-88373398,
E-mail: wyaoyu@nwu.edu.cn
[b] Department of Chemistry and Chemical Engineering, Yan'an University, Yan'an 716000, P. R. China

ligand in its amine form, or as a tridentate ligand in its deprotonated form.[15,16] In order to investigate the possible coordination modes of 2,3′-dipyridylamine compared to 2,2′-dipyridylamine, we explored the electronic effect of coordination atoms, the single-point energy calculations of four conformers of 2,3′-dipyridylamine based on the geometry of four conformers optimized by the DFT method. According to these guidelines, we used 2,3′-dipyridylamine as the ligand to coordinate with Ag^{I} and Cu^{II}, and obtained two 1D polymers with a helical or linear structure and one 2D supramolecule. Herein, we report the syntheses, crystal structures, and characterization of properties of ligand (**1**) and three complexes, namely $\{[Ag(L)_2]NO_3\}_n$ (**2**), $[Cu_2(L)_2(maa)_4]_n$ (**3**), and $[Cu(L)_4](ClO_4)_2 \cdot 2CH_3CH_2OH$ (**4**). At the same time, the magnetic properties of **3** have also been studied.

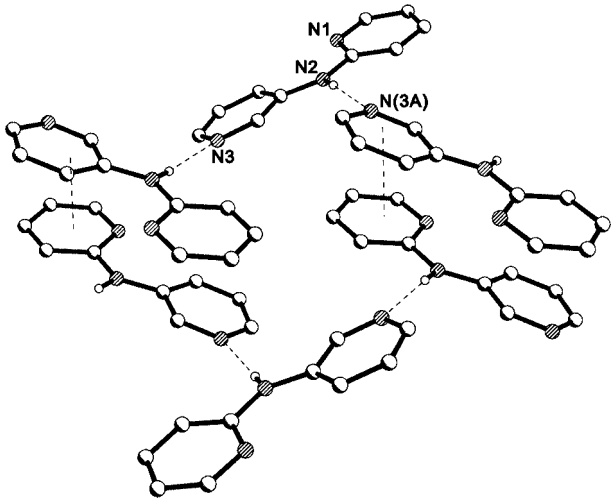

Figure 1. Perspective view of N–H···N hydrogen bonds and π-π stacking interactions in ligand **1**. [N2–N(3A) 3.0949(18) Å; N2–H···N(3A) 168.1(1)°; the distance between the centers of the pyridyl rings is 3.48(8) Å, the angle is 12.5427(4)° between two planes].

Results and Discussion

Description of the Structures

Ligand 1

The single-crystal X-ray structural analysis shows that ligand **1** crystallizes in an orthorhombic system. From the crystal structure of the ligand, it can be seen that the ligand forms zigzag chains in the solid state, and the molecules are held together by a series of N–H···N hydrogen bonds [N2–N(3A) 3.0949(18) Å; N2–H···N(3A) 168.1(1)°]. The two pyridine rings in the ligand are twisted with a dihedral angle of 12.5427(4)°, the ligand molecules are associated in pairs, in a head-to-tail arrangement showing π-π stacking interactions [the distance between the centers of the pyridyl rings is 3.48(8) Å, the dihedral angle is 12.5427(4)°], and give rise to a two-dimensional supramolecular structure (Figure 1).

In addition, single-point energy calculations and charge distributions for four conformers of the ligand have been carried out at DFT levels. Two stable and two less stable configurations have been obtained by structural optimization of the four conformers; the electronic layouts of the four conformers are shown in Figure 2. Single point energies of conformers (a), (b), (c), and (d) are –550.46003, –550.46214, –550.40317, and –550.40293 hartree, and the HOMO–LUMO energy gaps are 0.17477, 0.17273, 0.16899, and 0.16735 eV, respectively. These data reveal that configurations (a) and (b) are relatively more stable than (c) and (d). From the charge layouts of the four conformers, it can be seen that N1 and N3 each have an approximately equal donor electron ability in the four conformational isomers

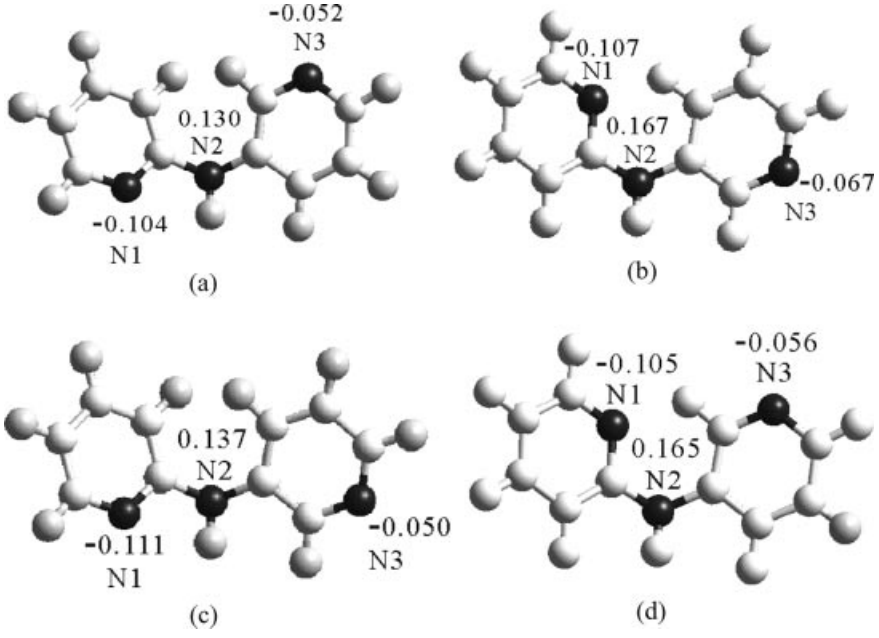

Figure 2. The four optimized conformations of the ligand **1**, as well as the calculated electron distributions.

(but each N1's donor electron ability is slightly stronger than that of each N3), if only considering their electronic effect.[17] However, we can see that the steric hindrance of N1 in configuration (b) and (d) is obviously larger than in configuration (a) and (c). Considering steric hindrance might affect the coordination ability of N1 in different configurations, we further investigated the coordination properties of ligand **1** with transition metal ions by experimental means. Fortunately, the experimental results prove this estimation. In the three synthetic complexes, we find that the ligand only takes on the coordination motifs of configuration (a) and (b). Configuration (b) presents in complex **4**, which combines with metal ions in a monodentate mode, and configuration (a) appears in polymers **2** and **3**, which links with metal ions in a bidentate bridging mode. Therefore, the difference in the coordination ability of N1 between configuration (a) and (b) mainly results from the difference in the steric hindrance of N1.

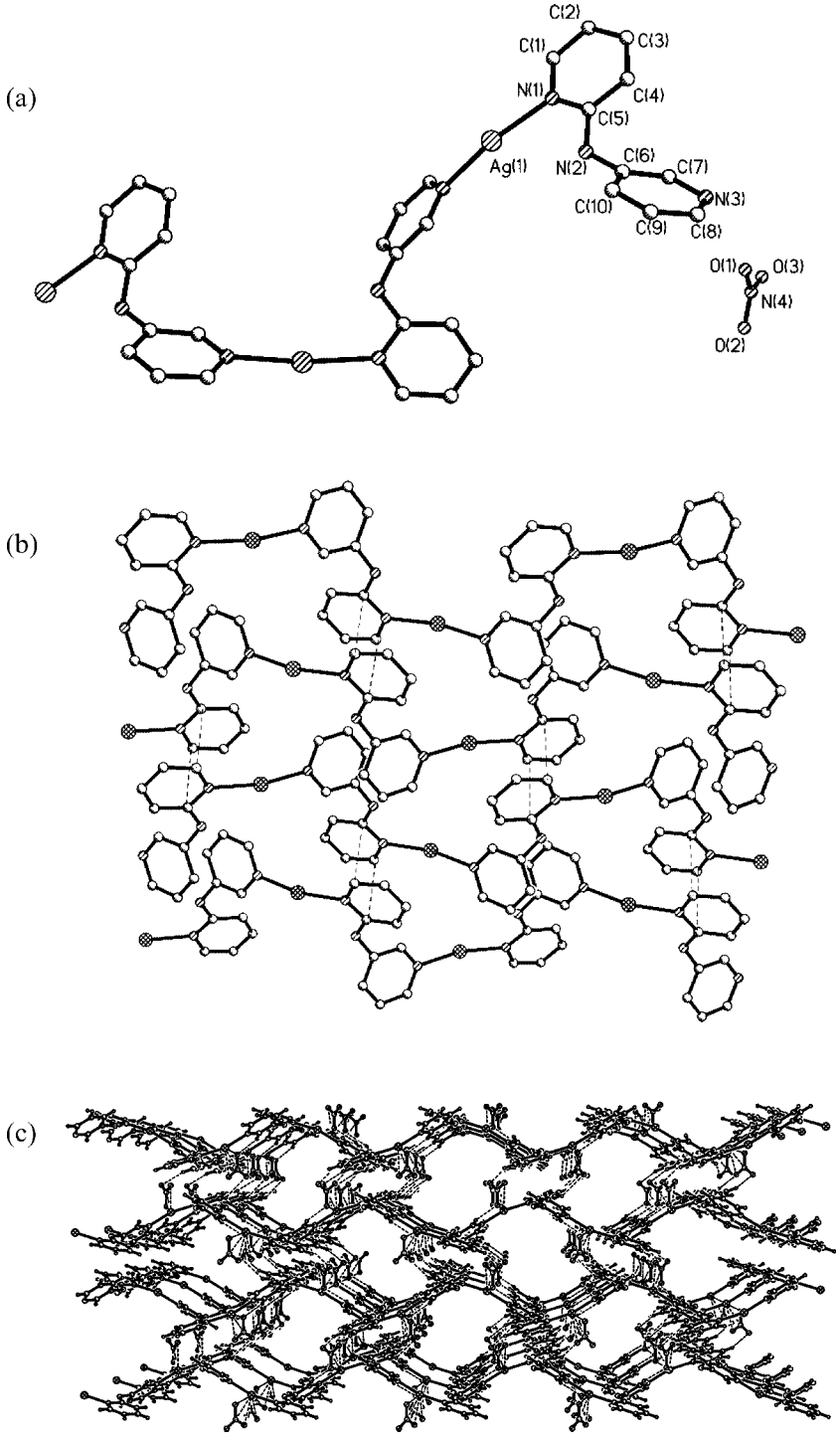

Figure 3. (a) The helical chain of **2**; (b) π-π packing interactions between helical chains; (c) the 3D structure formed by hydrogen-bonding and Ag···O weak interactions between adjacent layers.

{[Ag(L)$_2$]NO$_3$}$_n$ (2)

The single-crystal X-ray data shows the structure of **2** consists of one-dimensional (1D) cationic polymeric $\{[Ag(L)_2]\}^+_n$ chains and uncoordinated NO_3^- anions. The ligand adopts a *N*,*N*-bidentate bridging coordination mode by using two pyridine nitrogen atoms to coordinate to the Ag^I centers forming a 1D helical chain (Figure 3, a). The bond angle of N1–Ag1–N(3A) is 165.09(6)°, and the bond lengths of Ag1–N1 and Ag1–N(3A) are 2.193(2) and 2.196(2) Å, respectively, which are the typical values for Ag^I–N_{py} coordination distances.[18–21] The helices, parallel to the [010] direction, are generated around a twofold screw axis presented in the space group $P2_1/n$. Pyridine rings through centers of inversion from adjacent helical chains indicate significant π-π stacking interactions. Pyridine rings involving π-π stacking are absolutely parallel and the distances between their centroids are 3.769(6) and 3.593(8) Å, (Figure 3, b). Not only do the intermolecular π-π stacking interactions stabilize the helical frameworks but they also produce a two-dimensional layer parallel to the crystallographic *bc* plane, the same as most reported similar helical structures.[22,23]

A striking feature of **2** is the stacking pattern in the solid state. The packing diagram of **2** shows that the NO_3^- counterions are sandwiched between two layers, and every layer interacts with other close layers by two groups of C–H···O hydrogen bonds between uncoordinated oxygen atoms of NO_3^- and carbon atoms of the pyridine rings [C–O 3.310(2), 3.250(2) Å, C–H···O 146.63(1), and 150.35(3)°] and Ag···O weak interactions, resulting in a 3D supramolecular structure (Figure 3c).

[Cu$_2$(L)$_2$(maa)$_4$]$_n$ (3)

The structure of **3** consists of linear dinuclear one-dimensional polymeric $[Cu_2(L)_2(maa)_4]_n$ chains (Figure 4, a). The basal unit of the chain is a dinuclear Cu^{II} subunit of the paddle-wheel type, the two copper atoms are located at equivalent sites in the dinuclear unit. Each copper atom has a square pyramid coordination environment, with four oxygen atoms from four methacrylic groups, forming an equatorial plane, and one pyridyl nitrogen atom, occupying an axis place. The axial Cu–N distance is longer than the average Cu–O bond length. So the coordination geometry around the copper(II) atom can be regarded as a distorted square pyramid, and the Jahn–Teller effect in the polymer manifests itself as an asymmetric elongation along the axial direction. In the structure of **3**, four methacrylic acid groups are bound to the copper(II) atoms in the form of a symmetrical bridging mode (*syn*,*syn*-η^1:η^1:μ_2), thus forming a $Cu_2(maa)_4$ paddle-wheel type linked by L ligands. Just as those reported coordination polymers containing the paddle-wheel type,[24,25] the bridging ligand is located in an axial position in the paddle-wheel type structure. On the other hand, this big paddle-wheel type group hinders further torsion of the two pyridine rings of the bridging ligand, and

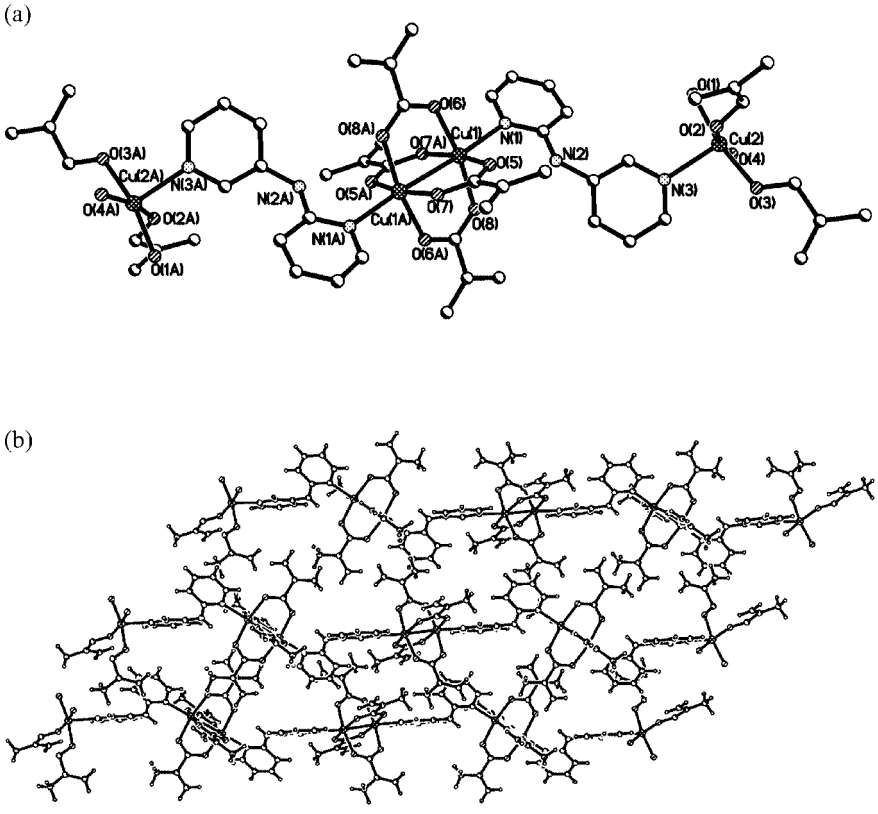

Figure 4. (a) Repeat units of the infinite coordination polymer of **3**; (b) The two-dimensional network of **3** viewed along the *a* axis.

causes the formation of a neutral one-dimensional linear chain rather than a helical chain. The chains self-organize and produce a two-dimensional supramolecular structure (Figure 4b) through C–H···O [C···O 3.513(5) Å, C–H···O 159.18(2)°] hydrogen bonds and C–H···π interaction [C–H···π 3.012(6) Å].

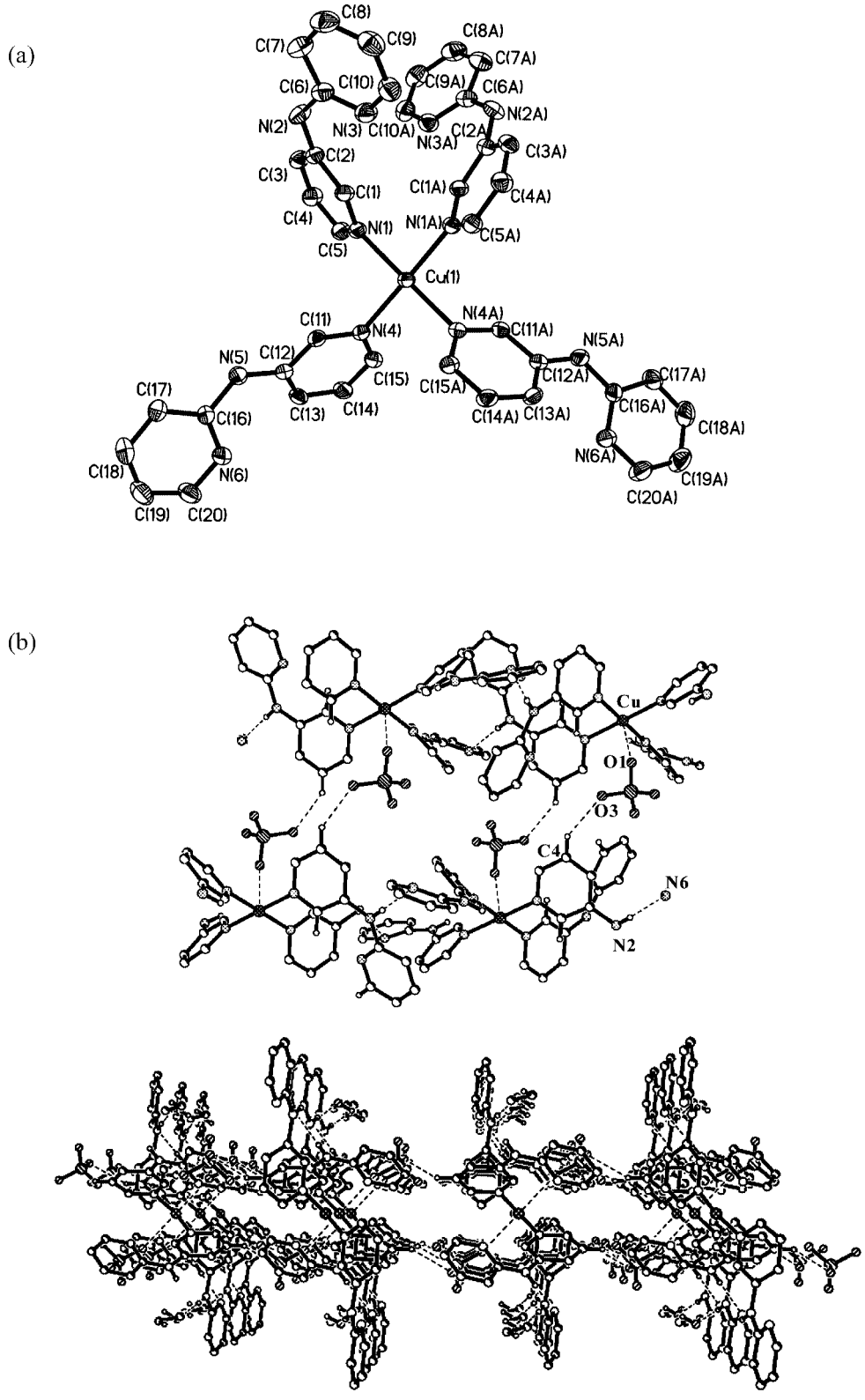

Figure 5. (a) ORTEP views showing the metal environment in the cation of **4**; (b) Perspective view of hydrogen-bonding and Cu–O weak interactions in **4** (top), and 2D packing view along the *b* axis (bottom).

[Cu(L)$_4$](ClO$_4$)$_2$·2CH$_3$CH$_2$OH (4)

Single-crystal X-ray diffraction analysis reveals that **4** is a neutral, mononuclear molecule with the Cu^{II} atom in a square coordination geometry with four pyridine nitrogen atoms of the four different dipyridylamine ligands (Figure 5, a). From the data about the N–Cu–N bond angles [89.14(14), 90.23(10), 90.23(10), and 90.42(13)°] and the Cu–N bond lengths [2.011(2), 2.011(2), 2.019(2), and 2.019(2) Å], it can be seen that the Cu^{II} ions together with the four nitrogen atoms form a perfect square geometry, and this ideal quadrangle structure is rare in the coordination geometry of Cu^{II}. A twofold rotary axis along the *b* axis direction presenting in space group *C*2/*c* is the typically symmetrical operation of **4**. The dihedral angles between two pyridine planes are about 28.106(2), 28.106(2), 23.418(2), and 23.418(2)° in the four ligands respectively, which are obviously larger than the free ligand **1**. This indicates that the ligand coordinated to the metal Cu^{II} promoted flexion of the σ_{C-N} bond. Interestingly, the four ligands all adopt a monodentate coordination mode and they all present in **4** as configuration (b), which further proves the theoretical judgment that the coordination ability of N1 atoms in configuration (b) has been reduced by a steric barrier. Two O atoms of the uncoordinated ClO_4^- anions form the acceptors of C(4)–H···O(3) [C–O 3.277(5) Å, C–H···O 140.36(2)°] intermolecular hydrogen bonds and Cu^{II}···O(1) weak interactions, which link the discrete units to form a 2D supramolecular structure together with the N(2)–H···N(6) [N–N 3.130(4) Å, N–H···N 176.69(3)°] intermolecular hydrogen bonds (Figure 5, b). In this complex, the uncoordinated ClO_4^- anions are an essential part of the structure, which act as a key linker in the 2D supramolecular structure, similar to BF_4^- in the reported complex $[(CH_3OH)_2Co(L)_4](BF_4)_4$.[26] However, the ethonal molecule present in complex **4** only functioned as an acceptor of intramolecular hydrogen bonds between the oxygen atoms of ethonal and amino nitrogen atoms of the ligand, which has little influence on the extended structure of complex **4**.

It is worth noting that **4** has a higher stability than the organic ligand owing to the fact that the single point energy (–2397.66179 hartree) of **4** is far lower than that of **1**. The HOMO–LUMO energy gap of **4** is 0.1332 eV, and the ligand has a high contribution to the front orbit of **4**. In addition, comparing this new ligand with 2,2′-dipyridylamine, we find that there are several differences between them: (i) 2,3′-dipyridylamine is a monodentate or bidentate ligand, and 2,2′-dipyridylamine is a chelate or monodentate ligand[27] in their amine form; (ii) 2,3′-dipyridylamine is an asymmetrical V-shaped molecule that may produce different conformers in complexes, and 2,2′-dipyridylamine is a symmetrical molecule that generally has three coordination modes, *syn-syn*, *syn-anti*, and *anti-anti*;[28] (iii) the *syn-syn* conformation of 2,2′-dipyridylamine builds many linear conformations of metal complexes in its deprotonated form,[29] and 2,3′-dipyridylamine can not form linear chains of metal atoms.

IR Spectra and TGA Analysis

IR spectra of the three complexes and the L ligand were recorded as KBr pellets in the range 4000–400 cm^{-1}. Ligand **1** shows a broad band at 3535 cm^{-1}, which can be assigned as the stretch absorption of ν(N–H). The next group of bands appears at 3071 cm^{-1}, corresponding to stretching vibrations of ν(C–H). Skeletal vibration of the pyridine ring shows a strong band at 1503 cm^{-1}. Because of the formation of intermolecular coordination bonds and hydrogen bonds, these absorption peaks are significantly shifted to lower frequencies in three complexes. In **2**, ν(N–H), ν(C–H), and the pyridine ring skeleton exhibit at 3448, 3017, and 1484 cm^{-1}, respectively; there is a strong absorption appearing at 1355.15 cm^{-1} for the noncoordinated anions of nitrate (NO_3^-). While in **3** the three characteristic peaks appear at 3526, 2923, and 1496 cm^{-1}. Another characteristic absorption for **3** is concerned with the values of asymmetric and symmetric stretching frequencies for the COO^- groups. The difference between ν_{as}(COO) and ν_s(COO) in comparison to the corresponding values in ionic species is currently employed to determine a characteristic coordination mode of the carboxylate group.[30] For **3**, the complex shows strong bands corresponding to ν_{as}(COO) and ν_s(COO) at 1601 and 1415 cm^{-1}, respectively. The $\Delta\nu$ is 186 cm^{-1}, close to the corresponding values for the sodium methacrylic (178 cm^{-1}), indicating that the methacrylic groups coordinate to metal ions in a symmetrical bridging mode (*syn*,*syn*-η^1:η^1:μ_2), in agreement with the paddle-wheel type structure of **3**. The IR spectra of **4** is similar to **2**, ν (N–H), ν (C–H), and the pyridine ring skeleton exhibit at 3621, 3206, and 1501 cm^{-1}, respectively. There is a slight red shift in **4** compared to **2** and **3** because of the more conjugated pyridine rings presenting in **4**. Meanwhile, a strong absorption band appears at 1131 cm^{-1} for the noncoordinated ClO_4^- anions. The bands appearing below 600 cm^{-1} may be assigned to the M–N frequencies for the three complexes.

The thermogravimetric analysis (TGA) reveals the weight loss of **2** occurs in two stages. The first stage occurs between 208.7 and 428.6 °C with a weight loss of 66.99%, which is equivalent to the loss of the ligands (calculated to be 66.83%). The total thermal effect of decomposition and oxidation of the ligand causes an exothermic peak at 216.5 C. When the temperature is above 440 °C, the $AgNO_3$ begins to decompose and metal silver is the final product, which constitutes 20.86% (calculated to be 20.93%). In contrast to **2**, the TGA shows that the weight of **3** remains almost unchanged from 40 to 180 °C. In the temperature range 180–400 °C, the complex undergoes a large weight loss of 76.67%, which represents weight loss from L and the methacrylic groups (calculated to be 79.12%). The DSC curve shows an exothermic peak at 218.4 °C, and the final product is CuO in 21.33% yield (calculated to be 20.88%). Complex **4** has undergone two steps of weight loss. The first weight loss occurs at 50–180 °C, corresponding to the loss of ethanol molecules. The higher temperature for the release of ethanol molecules is due to the strong hydrogen bonds involving ethanol molecules in

4. At this step, the experimental percentage weight loss is 8.01% (calculated to be 8.85%). The following steps of weight loss represent the pyrolysis of the organic ligand. The residues above 500 °C have a composition of CuO, and the observed residue percentage is 7.31% (calculated to be 7.69%).

Magnetic Properties

Variable-temperature magnetic susceptibility measurements over a 5–300 K range were carried out for **3**. The temperature dependence of magnetic susceptibilities χ_M and $\chi_M T$ of complex **3** is shown in Figure 6. It should be noted that polymer **3** exhibits two types of magnetic exchange interaction between two Cu^{II} ions; one is through short bridges via the methacrylic groups and the other is through a long bridge via L. Actually, because of the long L ligand fragment, the possibility of overlap of the magnetic orbital through the C and N atoms of L is negligible. Hence, the $Cu_2(maa)_4$ unit of paddle-wheel type plays an important role in the magnetic properties of polymer **3**. This type of antiferromagnetic interaction is strong because unpaired electron density from both Cu ions is transferred to the same orbital of the bridging methacrylic groups. The χ_M curve is typical for a very strong antiferromagnetic coupling with a small amount of paramagnetic impurities: the molar magnetic susceptibility decreases to a minimum and then suddenly increases when the temperature is lowered, attaining a maximum. The magnetic datafit to a Bleaney–Bowers equation,[31,32] which was derived from the spin Hamiltonian $H = -JS_1S_2$. The best-fit parameters are $-2J = 316\ cm^{-1}$, $g = 2.09$, and $R = 6.8 \cdot 10^{-4}$ ($R = \Sigma[(\chi_M T)_{obs} - (\chi_M T)_{calc}]^2/\Sigma[(\chi_M T)_{obs}]^{1/2}$). In contrast to the reported dinuclear Cu^{II} carboxylates, such as $Cu_2(C_{10}H_9O_2)_4(C_2H_5OH)_2$ ($-2J = 242\ cm^{-1}$),[33] $Cu_2(C_7H_{15}COO)_4$ ($-2J = 320\ cm^{-1}$), and $Cu_2(C_7H_{15}COO)_4(C_6H_7N)_2$ ($-2J = 300\ cm^{-1}$),[34] polymer **3** ($-2J = 316\ cm^{-1}$) shows a considerably stronger antiferromagnetic interaction.

Conclusions

In summary, a new V-shaped ligand **1** has been designed and synthesized. Density functional calculations at the B3LYP level of theory provide a satisfactory forecast for coordination properties of the ligand with metal ions. That is, two relatively stable conformers of the ligand combine with metal ions by different coordination modes. On the basis of ligand **1**, we have synthesized three novel complexes, $\{[Ag(L)_2]NO_3\}_n$ (**2**), $[Cu_2(L)_2(maa)_4]_n$ (maa = methacrylic acid) (**3**), and $[Cu(L)_4](ClO_4)_2 \cdot 2CH_3CH_2OH$ (**4**). Interestingly, polymers **2** and **3** assume a 1D helical structure and a linear framework, respectively, and **4** has a 2D supramolecular structure. Although the two relatively stable configurations of the ligand have very similar single-point energies and charge distributions, they form different coordination modes in the three complexes. These results indicate that the steric factors of the N atoms play important roles in the coordination modes of the dipyridylamine ligand, which may help us to understand the influence of organic spacers in determining the type and topology of the product.

Experimental Section

Physical Measurements: Elemental analyses (C,H,N) were determined with a Perkin–Elmer 240C elemental analyzer. Infrared spectra on KBr pellets were recorded with a Bruker EQUINOX-55 spectrometer in the range of 4000–400 cm^{-1}. Thermal analyses were performed with a Netzsch STA 449C microanalyzer with a heating rate of 10 °C·min^{-1} under air. Magnetic measurements were carried out on a polycrystalline sample with a SQUID magnetometer operating in the 5–300 K temperature range with an applied field of 5 kOe. Diamagnetic corrections were estimated from Pascal constants. ^1H NMR spectra were recorded with a Varian INOVA 400-MHz spectrometer. Electronic spectra were recorded with a Cary 300 Bio UV/Visible spectrophotometer. Mass spectra were obtained with a JEOL HX-110 HF double focusing spectrometer operating in the positive ion detection mode.

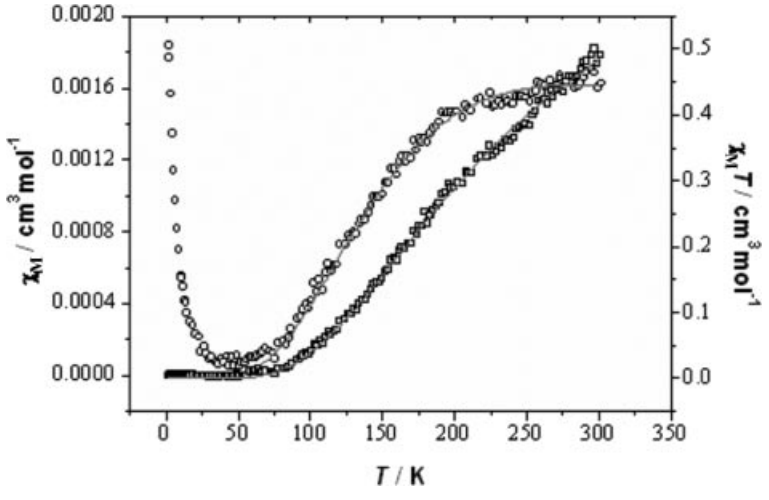

Figure 6. Plot of χ_M (○) (left scale) and $\chi_M T$ (□) (right scale) per Cu^{II} ion vs. T for **3**. The solid lines represent the best fit to the modified Bleaney–Bowers expression.

The Synthesis of Ligand 1: The reagents and solvents were purchased from commercial sources (Aldrich) and used as received. The 2,3′-dipyridylamine ligand was obtained as follows (Scheme 1): 2-aminopyridine (2.80 g, 34.8 mmol) and NaOBu (6.90 g, 72.9 mmol) were added to a 200 mL flask under nitrogen. Then the solution of 3-bromopyridine (3.44 mL, 34.8 mmol) and dry benzene (100 mL) were added to the container. The resulting solution was stirred for 72 h under reflux, and then cooled to room temperature. The original product was filtered and washed with dry benzene and water several times. The final product was purified by column chromatography on silica gel (dichloromethane/hexane, 1:1) to afford a colorless crystalline solid (4.16 g, 69.82%). $C_{10}H_9N_3$ (171.20): calcd. C 70.17, H 5.263, N 24.54; found C 69.98, H 5.210, N 24.66. IR (KBr): $\tilde{\nu}_{max}$ = 3535 (s), 3434 (s), 3294 (s), 3172 (s), 3071 (m), 3000 (m), 1643 (m), 1592 (m), 1503 (s), 1476 (s), 1421 (s), 1270 (m), 1210 (m), 1051 (s), 902 (m), 824 (m), 732.44 (s), 677 (m), 574 (w) cm^{-1}. UV/Vis (λ/nm): 320, 260, 220. MS (FAB): *m/z* (%) = 171.2 (L). ^1H NMR ($CDCl_3$): δ = 8.59 (s, 1 H, 1-H), 7.05 (s, 1 H, 2-H), 8.02 (d, 1 H, ^3J = 4.4 Hz, 3-H), 7.54 (dd, 1 H, ^3J = 5.8, ^3J = 5.4, 4-H), 7.27 (d, 1 H, ^3J = 5.8 Hz, 5-H), 6.80 (d, 2 H, ^3J = 6.3 Hz, 6-H), 8.25 (d, 2 H, ^3J = 3 Hz, 7-H) ppm.

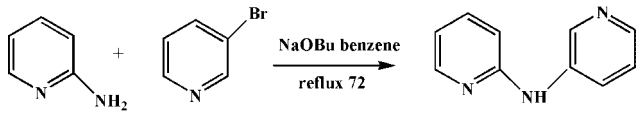

Scheme 1. The preparation of ligand 2,3′-dipyridylamine.

The Synthesis of the Complexes

The formation of **2**, **3**, and **4** with experimental conditions are shown in Scheme 2, their syntheses are given in the sequel.

{[Ag(L)$_2$]NO$_3$}$_n$ (2): A solution of silver(I) nitrate (16.9 mg, 0.1 mmol) in CH_2Cl_2 (10 mL) was added to a solution of L (17.1 mg, 0.1 mmol) in CH_2Cl_2 (10 mL). The reaction mixture was stirred at 25 °C for 1 h, and then the solvent was removed under reduced pressure. The resulting white powder was partially dissolved in acetonitrile (5 mL) (CH_3CN). The mixture was filtered,

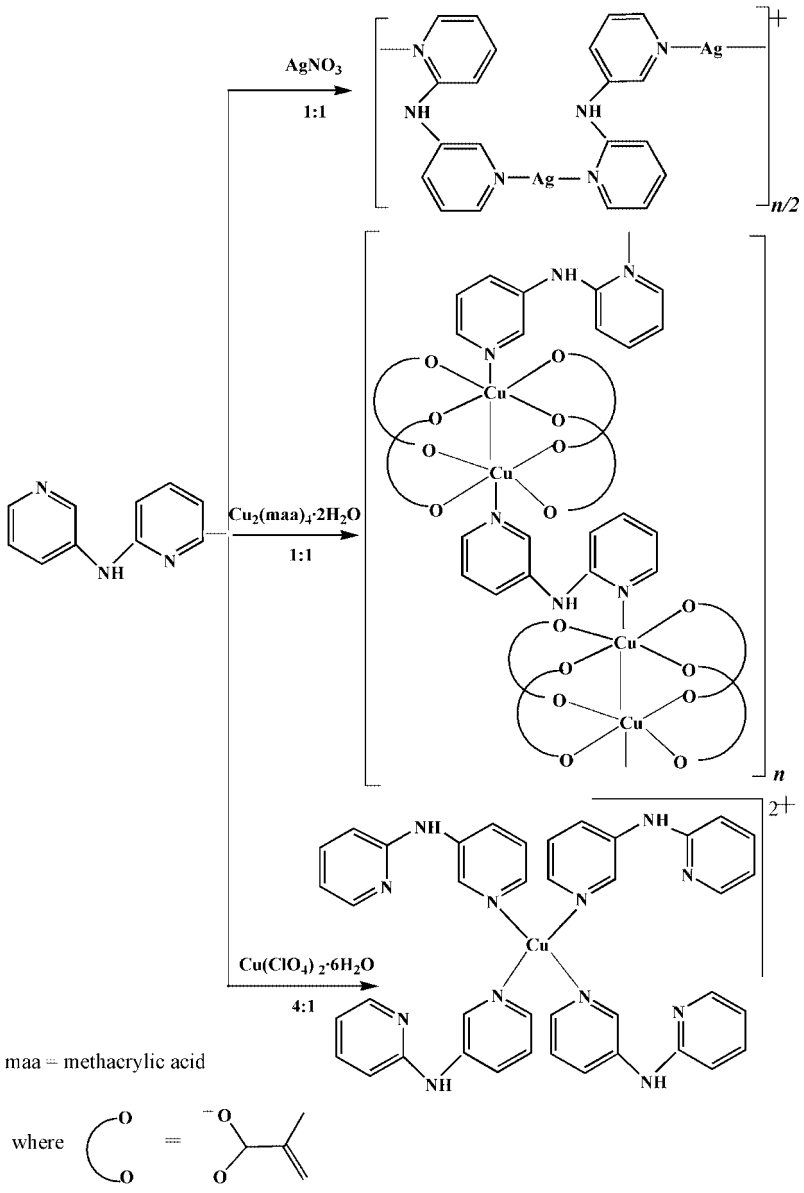

Scheme 2. The formation of **2**, **3**, and **4** with experimental conditions.

Table 1. Crystal data and structure refinements for **1**–**4**.

Complex	**1**	**2**	**3**	**4**
Empirical formula	$C_{10}H_9N_3$	$C_{10}H_8AgN_4O_3$	$C_{26}H_{29}Cu_2N_3O_8$	$C_{44}H_{48}Cl_2CuN_{12}O_{10}$
Formula mass	171.20	340.07	638.68	1039.38
Temperature [K]	273(2)	273(2)	273(2)	296(2)
Crystal system	orthorhombic	monoclinic	triclinic	monoclinic
Space group	*Pbca*	$P2_1/n$	$P\bar{1}$	$C2/c$
a [Å]	9.2018(3)	8.293(3)	9.092(8)	27.767(4)
b [Å]	11.9210(5)	14.174(4)	9.229(8)	10.7067(14)
c [Å]	15.6331(6)	9.751(3)	17.335(15)	18.144(2)
α [°]	90	90	93.786(13)	90
β [°]	90	101.064(5)	91.981(15)	115.891(9)
γ [°]	90	90	97.735(14)	90
V [Å^3]	1714.87(11)	1125.0(6)	1437(2)	4852.6(11)
Z	8	4	2	4
$D_{calcd.}$[g·cm^{-3}]	1.326	2.008	1.572	1.423
μ [mm^{-1}]	0.084	1.798	0.829	0.629
F [000]	720	668	714	21562
θ [°]	2.61–25.09	2.57–29.15	2.23–29.19	1.63–25.10
Data/restraints/parameters	1521/0/119	2769/0/164	6693/0/357	4315/0/314
Goodness-of-fit on F^2	1.043	1.045	0.999	1.073
R_1 wR_2[a] [$I > 2\sigma(I)$]	0.0417, 0.1069	0.0220, 0.0581	0.0455, 0.1268	0.0474, 0.1205

[a] $R_1 = \Sigma(||F_o| - |F_c|)/\Sigma|F_o|$; $wR_2 = [\Sigma w(F_o^2 - F_c^2)^2/\Sigma w(F_o^2)^2]^{1/2}$.

and diethyl ether vapor was diffused into this solution. After several days, suitable single crystals for X-ray diffraction could be obtained from the acetonitrile solution. Yield: 83.98% (28.56 mg). $C_{10}H_8AgN_4O_3$ (340.07): calcd. C 35.19, H 2.34, N 16.42; found C 35.13, H 2.40, N 16.67.

$[Cu_2(L)_2(maa)_4]_n$ (3): $Cu_2(maa)_4{\cdot}2H_2O$ was prepared according to a similar method reported previously in the literature.[35] A methanol solution (20 mL) of L (17.1 mg, 0.1 mmol) was slowly added to a solution of $Cu_2(maa)_4{\cdot}2H_2O$ (50.4 mg, 0.1 mmol) dissolved in methanol/ethanol (20 mL, v/v = 1:1). The resultant solution was allowed to evaporate slowly for several days at room temperature, and block-shaped green crystals of **1** were obtained. Yield: 66.82% (42.63 mg). $C_{26}H_{29}Cu_2N_3O_8$ (638.68): calcd. C 50.13, H 5.48, N 10.96; found: C 50.12, H 5.45, N 10.94.

$[Cu(L)_4](ClO_4)_2{\cdot}2CH_3CH_2OH$ (4): The solution of $Cu(ClO_4)_2{\cdot}6H_2O$ (37.05 mg, 0.1 mmol) in ethanol (10 mL) was carefully layered on top of a solution of L (68.4 mg, 0.4 mmol) in chloroform (10 mL) in a test tube. After several days at room temperature, yellow green single crystals appeared at the boundary between ethanol and chloroform with a yield of 63.66% (66.17 mg). $C_{44}H_{48}Cl_2CuN_{12}O_{10}$ (1039.38): calcd. C 50.85, H 4.65, N 16.17; found C 50.87, H 4.60, N 16.14.

Crystal Data Collection and Refinement: Diffraction experiments for **1**, **2**, **3**, and **4** were carried out with Mo-K_α radiation using a Bruker SMART APEXCCD diffractometer at 273(2) K for **1**, **2**, **3**, and 296(2) K for **4**. A summary of the crystallographic data and structure refinement is given in Table 1, and selected bond lengths and angles of the four complexes are listed in Table 2. All structures were solved by direct methods and refined with the full-matrix least-squares technique on F^2 using the SHELXS-97[36] and SHELXL-97[37] programs. All non-hydrogen atoms were refined anisotropically.

X-ray crystallographic data in CIF format for the structures reported in this paper have been deposited with the Cambridge Crystallographic Data Centre, CCDC-277949 (for **1**), -277950 (for **2**), -277951 (for **3**), and -294858 (for **4**). These data can be obtained free of charge from The Cambridge Crystallographic Data Centre via www.ccdc.cam.ac.uk/data_request/cif.

Table 2. Selected bond lengths [Å] and angles [°] for **1**–**4**.

Ligand **1**			
C(6)–N(3)	1.324(2)	C1–N(1)	1.329(2)
C(10)–N(3)	1.339(2)	C(5)–N(1)	1.350(2)
C(1)–N(2)–C(7)	129.87(13)		
Complex **2**			
Ag(1)–N(1)	2.193(2)	Ag(1)–N(3A)	2.196(2)
N(1)–Ag(1)–N(3A)	165.09(6)		
Complex **3**			
Cu(1)–O(7)A	1.960(3)	Cu(1)–O(8)	1.970(3)
Cu(1)–O(6)	1.964(3)	Cu(1)–O(5)	1.970(3)
Cu(1)–N(1)	2.193(3)	Cu(1)–Cu(1A)	2.6280(19)
Cu(2)–N(3)	2.183(3)	Cu(2)–Cu(2A)	2.6416(18)
O(7A)–Cu(1)–O(6)	89.64(12)	O(6)–Cu(1)–O(8)	168.32(10)
O(6)–Cu(1)–O(5)	90.33(12)	O(8)–Cu(1)–O(5)	88.27(12)
O(7A)–Cu(1)–N(1)	94.32(11)	O(6)–Cu(1)–N(1)	93.92(12)
O(4)–Cu(2)–N(3)	98.89(13)	O(1)–Cu(2)–N(3)	96.92(12)
O(3)–Cu(2)–N(3)	95.11(12)	O(2)–Cu(2)–N(3)	93.12(13)
Complex **4**			
Cu(1)–N(1)	2.011(2)	Cu(1)–N(1A)	2.011(2)
Cu(1)–N(4)	2.019(2)	Cu(1)–N(4A)	2.019(2)
N(1)–Cu(1)–N(1A)	89.14(14)	N(1)–Cu(1)–N(4)	90.23(10)
N(1A)–Cu(1)–N(4A)	90.23(10)	N(4)–Cu(1)–N(4A)	90.42(13)

Symmetry code: A: $x-1/2$, $-y+1/2$, $-z$ for **1**, $-x+3/2$, $y-1/2$, $-z+1/2$ for **2**, $-x+2$, $-y+2$, $-z$ for **3** and $-x+1$, y, $-z+3/2$ for **4**.

Calculation Details: The single-point energy and the orbit calculations based on the geometry of the free ligand and complex **4** were optimized by the DFT method using the B3LYP/LanL2DZ basis set in the Gaussian 03 program.[38] The data analyses were performed with Hyperchem 7.5 and GaussView 3.0.

Acknowledgments

This work was supported by the National Natural Science Foundation of China (Grant No. 20471048) and TRAPOYT.

[1] D. M. Shin, I. S. Lee, Y. K. Chung, *Inorg. Chem.* **2003**, *42*, 8838–8846.
[2] Z. B. Han, X. N. Cheng, X. M. Chen, *Cryst. Growth Des.* **2005**, *5*, 695–700.
[3] L. F. Anne-Marie, A. L. David, J. L. Paul, M. Z. Alexandra, D. B. Walker, *J. Am. Chem. Soc.* **2005**, *127*, 12612–12619.
[4] C. M. Zaleski, E. C. Depperman, C. D. Samara, M. Alexiou, D. P. Kessissoglou, M. L. Kirk, *J. Am. Chem. Soc.* **2005**, *127*, 12862–12872.
[5] B. Moulton, J. Lu, M. J. Zaworotko, *J. Am. Chem. Soc.* **2001**, *123*, 9924–9925.
[6] B. E. Villarroya, C. Tejel, M. M. Rohmer, O. A. Luis, *Inorg. Chem.* **2005**, *44*, 6536–6544.
[7] C. Y. Su, Y. P. Cai, C. L. Chen, M. D. Smith, W. Kaim, H. C. Loye, *J. Am. Chem. Soc.* **2003**, *125*, 8595–8613.
[8] Y. L. Jack, A. R. Karren, N. Christine, *Inorg. Chem.* **2001**, *40*, 4516–4517.
[9] H. Gudbjartson, K. Biradha, K. M. Poirier, M. J. Zaworotko, *J. Am. Chem. Soc.* **1999**, *121*, 2599–2600.
[10] K. Biradha, C. Seward, M. J. Zaworotko, *Angew. Chem. Int. Ed.* **1999**, *38*, 492–495.
[11] C. L. Chen, H. Y. Tan, J. H. Yao, C. Y. Su, *Inorg. Chem.* **2005**, *44*, 8510–8520.
[12] R. H. Wang, L. J. Xu, X. S. Li, Y. M. Li, M. C. Hong, A. S. C. Chan, *Eur. J. Inorg. Chem.* **2004**, 1595–1599.
[13] X. M. Chen, G. F. Liu, *Chem. Eur. J.* **2002**, *8*, 4811–4817.
[14] C. H. Zhou, H. Y. Zhu, Y. Y. Wang, D. S. Li, Q. Z. Shi, *J. Mol. Struct.* **2005**, *779*, 61–67.
[15] Y. J. Kang, C. Seward, D. T. Song, S. N. Wang, *Inorg. Chem.* **2003**, *42*, 2789–2797.
[16] M. M. Rohmer, M. Be'nard, *J. Am. Chem. Soc.* **1998**, *120*, 9372–9373.
[17] Y. B. Xie, J. R. Li, C. Zhang, X. H. Bu, *Cryst. Growth Des.* **2005**, *5*, 1743–1749.
[18] V. J. Catalano, M. A. Malwitz, A. O. Etogo, *Inorg. Chem.* **2004**, *43*, 5714–5724.
[19] D. A. McMorran, P. J. Steel, *Chem. Commun.* **2002**, 2120–2121.
[20] M. C. Hong, Y. J. Zhao, W. P. Su, R. Cao, M. Fujita, Z. Y. Zhou, A. S. C. Chan, *Angew. Chem. Int. Ed.* **2000**, *39*, 2468–2470.
[21] D. A. McMorran, P. J. Steel, *Chem. Commun.* **2002**, 2120–2121.
[22] G. H. Cui, J. R. Li, J. L. Tian, X. H. Bu, S. R. Batten, *Cryst. Growth Des.* **2005**, *5*, 1775–1780.
[23] H. L. Zhu, Y. X. Tong, X. M. Chen, *J. Chem. Soc., Dalton Trans.* **2000**, 4182–4186.
[24] X. J. Luan, Y. Y. Wang, L. J. Zhou, C. H. Zhou, Q. Z. Shi, *J. Mol. Struct.* **2005**, *750*, 63–68.
[25] M. Taybani, K. Feghali, S. Gambrotta, G. P. A. Yap, *Inorg. Chem.* **2001**, *40*, 1399–1401.
[26] H. Amouri, L. Mimassi, M. N. Rager, B. E. Mann, C. Guyard-Duhayon, L. Raehm, *Angew. Chem.* **2005**, *117*, 4619–4622; *Angew. Chem. Int. Ed.* **2005**, *44*, 4543–4546.
[27] S. Kar, N. Chanda, S. M. Mobin, F. A. Urbanos, R. J. Aparicio, G. K. Lahiri, *Inorg. Chem.* **2005**, *44*, 1571–1579.
[28] J. T. Sheu, C. C. Lin, I. Chao, C. C. Wang, S. M. Peng, *Chem. Commun.* **1996**, 315–316.
[29] F. A. Cotton, L. M. Daniels, C. A. Murillo, I. Pascual, *J. Am. Chem. Soc.* **1997**, *119*, 10223–10224.
[30] G. B. Deacon, R. J. Phillips, *Coord. Chem. Rev.* **1980**, *33*, 227–238.
[31] B. Bleaney, K. D. Bowers, *Proc. R. Soc. London, Ser. A* **1952**, *214*, 451–465.
[32] O. Kahn, *Molecular Magnetism*, VCH, Weinheim, Germany, **1993**.
[33] F. P. W. Agterberg, H. A. J. Provo Kluit, W. L. Driessen, H. Oevering, W. Buijs, M. T. Lakin, A. L. Spek, J. Reedijk, *Inorg. Chem.* **1997**, *36*, 4321–4328.
[34] C. C. Hadjikostas, G. A. Katsoulos, M. P. Sigalas, C. A. Tsipis, *Inorg. Chim. Acta* **1990**, *67*, 165–168.
[35] Y. Y. Wang, Q. Shi, Q. Z. Shi, Y. C. Gao, Z. Y. Zhou, *Chin. Sci. Bull.* **1998**, *43*, 2512–2516.
[36] G. M. Sheldrick, *SHELXS 97*, Program for Crystal Structure Solution, University of Göttingen, Germany, **1997**.
[37] G. M. Sheldrick, *SHELXL 97*, Program for Crystal Structure Refinement, University of Göttingen, Germany, **1997**.
[38] M. J. Frisch, G. W. Trucks, H. B. Schlegel, G. E. Scuseria, M. A. Robb, J. R. Cheeseman, V. G. Zakrzewski, J. A. Montgomery, R. E. Stratmann, J. C. Burant, S. Dapprich, J. M. Millam, A. D. Daniels, K. N. Kudin, M. C. Strain, O. Farkas, J. Tomasi, V. Barone, M. Cossi, R. Cammi, B. Mennuci, C. Pomelli, C. Adamo, S. Clifford, J. Ochterski, G. A. Petersson, P. Y. Ayala, Q. Cui, K. Morokuma, D. K. Malick, A. D. Rabuck, K. Raghavachari, J. B. Foresman, J. Cioslowski, J. V. Oritz, B. B. Stefanov, G. Liu, A. Liashenko, P. Piskorz, I. Komaromi, R. Gomperts, R. L. Martin, D. J. Fox, T. Keith, M. A. Al-Laham, C. Y. Peng, A. Nanayakkara, C. Gonzalez, M. Challacombe, P. M. W. Gill, B. G. Johnson, W. Chen, M. W. Wong, J. L. Andres, M. Head-Gordon, E. S. Replogle, J. A. Pople, *GAUSSIAN03, Revision C.02*; Gaussian, Inc., Pittsburgh, PA, **2003**.

Received: January 18, 2006
Published Online: April 20, 2006

